processes

MDPI

Article

Failure Risk Prediction Model for Girth Welds in High-Strength Steel Pipeline Based on Historical Data and Artificial Neural Network

Ke Wang [1,2], Min Zhang [1,*], Qiang Guo [3], Weifeng Ma [2], Yixin Zhang [4] and Wei Wu [4]

[1] School of Materials Science and Engineering, Xi'an University of Technology, Xi'an 710048, China; wangke003@cnpc.com.cn
[2] Tubular Goods Research Institute of CNPC, Xi'an 710077, China; mawf@cnpc.com.cn
[3] Shaanxi City Gas Industry Development Co., Ltd., Xi'an 710048, China; 18049688165@163.com
[4] School of Chemical Engineering, Northwest University, Xi'an 710069, China; zh_angyixin@163.com (Y.Z.); wuwei@nwu.edu.cn (W.W.)
* Correspondence: zhmmn@xaut.edu.cn

Abstract: Pipelines are the most economical and sensible way to transport oil and gas. Long-distance oil and gas pipelines consist of many steel pipes or pipe fittings joined by welded girth welds, so girth welds are an essential part of pipelines. Owing to the limitations of welding conditions and the complexity of controlling weld quality in the field, some defects are inevitably present in girth welds and adjacent weld areas. These defects can lead to pipeline safety problems; therefore, it is necessary to perform failure risk assessment of pipeline girth welds. In this study, an artificial neural network model was proposed to predict the failure risk of pipeline girth welds with defects. Firstly, many pipeline girth weld failure cases, pipeline excavation, and inspection data were collected and analyzed to determine the main factors influencing girth weld failure. Secondly, a spatial orthogonal optimization method was used to select training samples for the artificial neural network model to ensure that the training sample set could cover the feature space with a minimum number of samples. Thirdly, a prediction model based on BP neural networks was established to predict the failure risk levels. The training dataset/testing dataset was 602/4215, and the prediction accuracy for all risks of girth welds achieved an acceptable level. This study can provide a valuable reference for pipeline operators to prevent pipeline accidents.

Keywords: pipeline; girth welds; sample selection; failure risk

Citation: Wang, K.; Zhang, M.; Guo, Q.; Ma, W.; Zhang, Y.; Wu, W. Failure Risk Prediction Model for Girth Welds in High-Strength Steel Pipeline Based on Historical Data and Artificial Neural Network. *Processes* **2023**, *11*, 2273. https://doi.org/10.3390/pr11082273

Academic Editor: Jie Zhang

Received: 21 June 2023
Revised: 24 July 2023
Accepted: 24 July 2023
Published: 28 July 2023

1. Introduction

Oil and natural gas are the most common energy sources. Compared with railway and road transportation, pipelines are still the safest and most efficient oil and gas transportation mode. However, with increasing energy demand, more and more long-distance oil and gas pipelines are being used [1–5]. Long-distance pipelines consist of a large number of steel pipes or fittings connected by girth welds formed by welding, including arc welding [6], manual welding, fully automatic welding, etc.

Owing to the limitations of welding technical conditions and the complex control of field construction quality, various welding defects, such as cracks, air holes, slag inclusion, incomplete fusion, and excessive residual stress [7], are inevitable in the girth welds and the adjacent weld areas [8–10]. Under the service conditions, girth welds may become a relatively weak part in pipeline structures, which are easy to crack or even break, causing a large amount of leakage of oil and natural gas and sudden and catastrophic accidents, such as fires and explosions [11]. The causes of pipeline girth weld failure include poor welding quality, corrosion and corrosion fatigue, third-party damage, soil movement, and so on. The Myanmar–China pipeline once leaked and exploded due to the weak quality of

girth welds, resulting in 24 people being injured. It is urgent that the safety risks of pipeline girth welds are investigated, and the existing investigation is mainly based on the results of internal the inspection of magnetic flux leakage, negative reassessment, and directional sampling. However, the length of China's pipelines exceeds 40,000 km and there are more than 3 million welds, so the workload is large and high-risk welds cannot be effectively found.

At present, many studies have focused on the failure prediction of pipelines, including failure risk [12], failure probability and reliability [13], failure consequences [14], failure types [15], failure rate [16], failure pressure [17,18], and others. These include qualitative, quantitative, and semi-quantitative assessment methods. For instance, Markovki and Mannan [19] developed risk-assessment methods for oil and gas pipelines through fuzzy logic and fuzzy rule-based systems. Shahria and Sadiq [20] developed a sustainability assessment method based on fuzzy tie analysis for oil and gas pipeline risk analysis.

As computing power continues to advance, researchers are showing growing interest in computer simulation and intelligent approaches. Within the safety risk field, machine learning methods have received widespread application. Kumari [21] developed a comprehensive risk prediction model. They selected the influencing factors and established an artificial neural network model to predict the causes and consequences of accidents, according to the importance of corrosion-induced pipeline accidents. Ren [22] developed a BPNN prediction model using the mileage, height difference, inclination angle, pressure, and Reynolds number of a natural gas pipeline as input parameters and the maximum average corrosion rate of the pipeline as the output parameter. The results showed that the model had good fitting accuracy and prediction results. Li [23] established an improved SVR model to predict subsea crude oil pipeline corrosion effectively. The model will serve as a valuable online tool to support the safety and digitalization of process systems. Cai et al. [24] used ANN, SVM, and linear regression to develop a prediction model of the strength of pipes containing corrosion defects. However, all these studies focused on whole pipes, rather than welds.

For girth welds, Chang [25] used a numerical simulation method based on the Gurson–Tvergaard–Needleman (GTN) model to analyze the crack initiation and dynamic fracture behavior of a welded pipe under pure bending load. Wu et al. [26]. investigated the effects of the crack size, pipe diameter–thickness ratio, and material parameters on the fracture assessment accuracy of pipe girth welds based on the failure assessment diagram theory and the equivalent stress–strain relationship method. He [27] established a numerical simulation model of the stress-induced magnetic signal of a girth weld with unequal wall thickness and used the model to calculate and analyze the quantitative variation law of the magnetic gradient signal of a girth weld. The current studies on girth welds focus on the failure mechanism, detection and evaluation, and repair technology, with some research on failure risk prediction. Fortunately, a large amount of data on girth weld construction, operation, failure, and testing accumulated during the construction and operation of pipelines, which provides strong support for the further study of the risk prediction of pipeline girth welds [28,29].

This study uses a large amount of collected girth weld failure data to conduct risk prediction model research. The focus is on (1) the identification of failure factors of oil and gas pipeline girth welds; (2) the use of a spatially orthogonal optimal method to purposefully select samples with an extreme imbalance in data distribution; and (3) the use of artificial neural networks to construct a pipeline girth weld failure risk prediction model.

The remainder of this paper is organized as follows: Section 2 focuses on the collection and preprocessing of pipeline girth weld failure data. Section 3 proposes a sample data selection method based on a spatially orthogonal optimal method. Section 4 describes the construction of the failure risk prediction model based on a neural network. In Section 5, influence factor analysis, model prediction performance, and sensitivity analysis are carried out. Section 6 concludes the paper.

2. Data Collection and Preprocessing

2.1. Data Sources

According to pipeline girth weld failure cases and field inspection data, a lot of girth failure sample data in this study were collected. These samples were classified into three risk levels, high, medium, and low, based on the service conditions of the welds. The samples that failed or required replacement were defined as high-risk welds, those that required repair, rather than replacement, were defined as medium-risk welds, and others as low-risk. It was found that most of the available data samples focused on X70 and X80 steel pipes; therefore, the prediction model was applied to these two pipe types. Table 1 shows the basic information of the samples.

Table 1. The numbers and risk levels of the collected raw girth weld samples.

Risk Level	Data Sources	Number	X70 Steel Number	X70 Steel Proportion	X80 Steel Number	X80 Steel Proportion	X70 and X80 Proportion
High risk	Failed welds	86	15	17%	29	34%	51%
Medium risk	Excavation and repair of welded joints	2905	313	11%	2039	79%	90%
Low risk	Excavation without repair of welded joints	24,773	4365	18%	17,140	69%	87%

2.2. Influencing Factors and Normalization

Many factors affect the failure risk of girth welds in oil and gas transmission pipelines, but the industry generally agrees that the three key factors are the pipe materials and properties, weld defects, and loads [26,30]. Based on the samples collected, the factors that cause girth weld failures can be divided into three categories: pipe type and performance-related indicators, defect-related indicators, and load-related indicators. Table 2 shows the details of the indicators and their normalization. There are 20 specific indicators of girth weld failure risk. These indicators need to be normalized to make them valid training samples for machine learning models. Some of these factors, such as the welding process, repair, and defect type, are Boolean or enumerated types and require special normalization methods, as shown in Table 2.

Figure 1 shows the effects of some main factors on the failure of the pipeline girth welds. From Figure 1a, it can be found that the percentage of girth weld failures for pipe diameters above 900 mm was 36%, 26% for pipe diameters from 600 mm to 900 mm and 300 mm to 600 mm, and 12% for pipe diameters below 300 mm. Figure 1b provides the relationship between failed girth welds and wall thickness, and it can be seen that, in all failure cases, the percentage of pipes with wall thicknesses of 10 mm and above was 65%, while the percentage of those with wall thicknesses below 10 mm was 35%. Eighty-three percent of the girth weld defects were located in the root of the welds (Figure 1c). Figure 1d provides the circumferential distribution of defects; 48% of the defects were at the top of the pipe (10 o'clock–2 o'clock) and 48% at the bottom of the pipe (4 o'clock–8 o'clock).

Table 2. The indicators affecting the failure risks of the girth welds of pipelines.

Level I Indicators	Level II Indicators	Symbol	Parameter	Normalization Method
Pipe material and performance	Steel grade	X1	X70; X80	X70: 0 X80: 1
	Diameter	X2	D	(D–1016)/(1219–1016)
	Wall thickness	X3/X4	$t1$; $t2$	(t–18.4)/(50–18.4)
	Yield strength	X5	σ	(σ–485)/(700–485)
	Toughness	X6	CVN	(CVN–20)/(300–20)
	Welding process	X7	Semi-automatic welding (SAW); Manual welding (MW); Fully automatic welding (FAW)	SAW: 1 MW: 0.5 FAW: 0
	Construction in winter or not	X8	Yes or No	Yes: 1 No: 0
	Repaired or not	X9	Yes or No	Yes: 1 No: 0
	Joint or not	X10	Yes or No	Yes: 1 No: 0
	Fixed joint of not	X11	Yes or No	Yes: 1 No: 0
Welding defect	Defect Type	X12	Volumetric; Planar; Cracked	Cracked: 1 Planar: 0.5 Volumetric: 0
	Defect position along the depth direction	X13	Outer surface; Interlayer; Root	Root: 1 Outer surface: 0.5 Interlayer: 0
	Defect position along the circumference	X14	S	2–4 and 8–10:1 10–2:0.5 4–8:1
	Defect length	X15	L	$L/\pi D$
	Defect height	X16	a	$a/t2$
	Weld radiographic grade	X17	H	$H/4$
Loading	Pressure	X18	P	$P/12$
	Axial stress	X19	Fixed joint; Elbow/Bend; Normal	Fixed joint: 1 Elbow/Bend: 0.5 Normal: 0
	Geological area	X20	Located in a geologically hazardous area	Yes: 1 No: 0

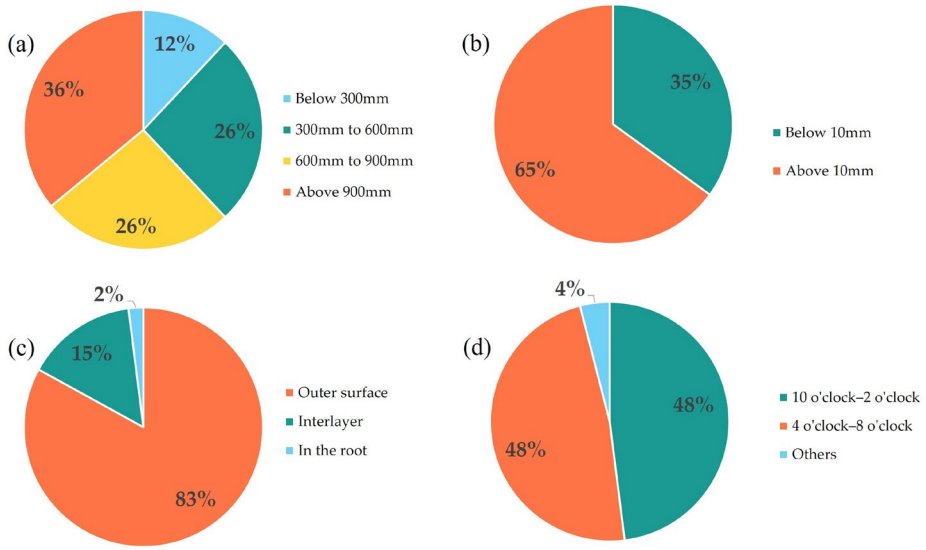

Figure 1. The effects of some main factors on the failure of the pipeline girth welds. (**a**) Relationship between failed girth welds and pipe diameter. (**b**) Relationship between failed girth welds and wall thickness. (**c**) Relationship between failed girth welds and location in the weld. (**d**) Relationship between failed girth welds and circumferential distribution of defects.

2.3. Sample Extraction and Screening

According to the field data sources and the definitions of high-, medium-, and low-risk samples, the format of each collected data sample was standardized. As many samples in the original dataset were incomplete, it was necessary to clean and preprocess them to obtain usable samples. The principle was that each data sample was complete, and the outlier points in the data needed to be excluded during data cleansing and pre-processing. After that, a total of 44 high-risk, 1823 medium-risk, and 2950 low-risk samples were extracted and sorted, as shown in Table 3. Table 4 shows examples of the girth weld samples.

Table 3. The samples extracted from the raw data.

Risk Level	Source	Welds from X70 Steel Pipelines	Welds from X80 Steel Pipelines
High risk	Failure analysis	13	7
	Cutting treatment	2	22
Medium risk	B-type sleeve	179	236
	Epoxy sleeve	14	464
	Composite material	30	866
	Polishing treatment	7	27
Low risk	Level 1 weld junction	53	590
	Level 2 weld junction	155	1863
	Level 3 weld junction	29	251
	Level 4 weld junction	0	9
Total	/	482	4335

Table 4. The examples of the girth weld samples.

X1	X2	X3	X4	X5	X6	X7	X8	X9	X10	X11	X12	X13	X14	X15	X16	X17	X18	X19	X20	Risk Level
X80	1219	18.4	555	60	SAW	No	18.4	No	No	No	Cracked	Root	6.33	23.5	0.9	4	12	Elbow/Bend	No	High
X80	1219	15.3	555	60	SAW	No	18.4	Yes	Yes	No	Cracked	Root	5.8	35	2.7	4	12	Elbow/Bend	No	High
X80	1219	18.4	555	60	SAW	Yes	22	No	No	No	Cracked	Root	6	64	3.5	4	12	Elbow/Bend	No	High
X80	1219	18.4	555	60	SAW	No	18.4	No	No	No	Cracked	Root	2.81	20	1	4	12	Elbow/Bend	No	High
X80	1219	18.4	555	60	SAW	Yes	18.4	No	No	No	Cracked	Root	6	38	9.3	4	12	Normal	No	High
X80	1219	16.5	555	60	FAW	No	16.5	No	No	No	Planar	Root	0.75	70	10	4	12	Normal	No	High
X70	1016	15.3	555	60	SAW	No	15.3	No	No	No	Cracked	Root	4	48	0.2	4	10	Normal	No	High
X70	1016	15.3	555	60	SAW	No	15.3	No	No	No	Planar	Root	11.94	39	2.67	4	10	Normal	No	Medium
X70	1016	18.4	555	60	SAW	No	18.4	No	No	No	Planar	Root	4.78	65	2.8	4	10	Normal	No	Medium
X70	1016	15.3	555	60	SAW	No	17.5	Yes	No	No	Planar	Outer surface	6.96	220	2.94	4	10	Elbow/Bend	No	Medium
X80	1219	18.4	555	60	MW	No	18.4	No	Yes	No	Planar	Outer surface	5.58	40	1.5	4	12	Normal	No	Medium
X80	1219	18.4	555	60	MW	No	18.4	No	No	No	Volumetric	Root	2.78	60	2	4	12	Elbow/Bend	No	Medium
X80	1219	22	555	60	MW	No	22	No	No	No	Planar	Root	8.46	17	2.86	4	12	Elbow/Bend	No	Medium
X80	1219	18.4	555	60	SAW	No	18.4	No	No	No	Planar	Root	0.05	8	2.4	4	12	Normal	No	Medium
X80	1219	18.4	555	60	MW	No	18.4	No	Yes	No	Volumetric	Interlayer	3.95	4	1.2	2	12	Elbow/Bend	No	Low
X80	1219	18.4	555	60	MW	No	18.4	No	No	No	Volumetric	Interlayer	6.27	0.9	1.1	1	12	Elbow/Bend	No	Low
X80	1219	18.4	555	60	MW	No	18.4	No	No	No	Volumetric	Interlayer	0.97	8	1.7	2	12	Normal	No	Low
X80	1219	18.4	555	60	MW	No	18.4	No	No	No	Volumetric	Interlayer	0	0	0	1	12	Normal	No	Low
X70	1016	18.4	555	60	SAW	No	18.4	No	No	No	Volumetric	Interlayer	9.47	7	1.2	2	10	Normal	No	Low
X70	1016	15.3	555	60	SAW	No	18.4	No	No	No	Volumetric	Interlayer	7.03	4	1.2	2	10	Normal	No	Low
X70	1016	15.3	555	60	SAW	No	15.3	No	No	No	Volumetric	Interlayer	11.75	3	1.1	1	10	Normal	No	Low

3. Selection of Training Samples

From the screened samples it, can be seen that there was a serious imbalance between the various types of risk welds. The number of high-risk welds was only 44, while the number of low-risk welds was almost 3000, with huge differences between the numbers of welds of different risk levels. Whether linear regression or traditional neural network training with randomly selected samples was used, the prediction results would be heavily biased toward the higher number of risk types. To address this challenge, this study proposed a spatially orthogonal optimal method for the targeted selection of training samples.

Mathematically, it should be possible to successfully train a neural network using training samples that contain most of the feature information and have minimal overall linear correlation. Ideally, the training samples should be orthogonal to each other, so that the training sample set can contain the maximum number of features with the minimum number of samples. Therefore, the mathematical model for training sample set selection can be expressed as Equation (1).

$$\min C = \sum_{i \in J; j \in J} V_i \cdot V_j \tag{1}$$

where J is the set of sample vector numbers in the training set and V_i is the i-th sample vector. The solution objective of Equation (1) is J. Owing to the large number of samples, it was difficult to produce a training set with the minimum overall linear correlation by conventional methods. Therefore, this study proposes a training set selection algorithm based on a heuristic method to achieve the overall correlation minimum. First, the sample vector correlation matrix C (Equation (2)) could be constructed based on the sample vectors.

$$\mathrm{C} = \begin{bmatrix} V_1V_1 & V_1V_2 & \dots & V_1V_n \\ V_2V_1 & V_2V_2 & \dots & V_2V_n \\ \dots & \dots & \dots & \dots \\ V_nV_1 & V_nV_2 & \dots & V_nV_n \end{bmatrix} \tag{2}$$

Let $d_{ij} = V_iV_j$; then, the algorithm for selecting the minimum correlation sample set can be described as follows:

(1) Construct a set $A\ Set = \{d_{ij} | 1 \le i; i < j \le N\}$ and let $J = \{\}$. Determine the number of training samples K;

(2) Search the smallest element $d_{i_{min}j_{min}}$ in $ASet$ and add its subscript (i_{min}, j_{min}) to J, then delete this element from $ASet$;

(3) Determine whether the number of elements in J (K_N) is greater than or equal to K, and if $K_N \ge K$, proceed to step (4); otherwise, proceed to step (2);

(4) Determine the corresponding V_{i_m} as the training sample based on the subscripts of J.

4. Establishment of Failure Risk Prediction Model

4.1. Prediction Model Selection

The results of the girth weld failure risk prediction were divided into three categories: "high risk", "medium risk", and "low risk". This means that risk prediction was actually solving Equation (3).

$$r = \mathrm{g}(c_0, c_1, \dots, c_{m-1}) \tag{3}$$

where $c_0, c_1, \dots, c_{m-1}$ represent the corresponding indicators in Table 2. g is a mapping relationship. r is the predicted result.

Owing to the complexity of the factors influencing the failure risk of girth welds, it is extremely challenging to build a rigorous mathematical model to predict weld failure risk. Machine learning is a potential alternative method because it can effectively mine internal relationships and patterns from data. There are various methods for machine learning, such as neural networks, support vector machines, and random forests. Artificial neural networks (ANNs) [31,32] have powerful nonlinear mapping capability to analyze any specific task, such as classification, prediction, and control, so it is a feasible approach to construct an ANN-based girth weld failure prediction model using the collected actual data.

In this study, a fully connected BP neural network was selected as the network architecture for girth weld failure risk prediction. The general framework of the research methodology is shown in Figure 2.

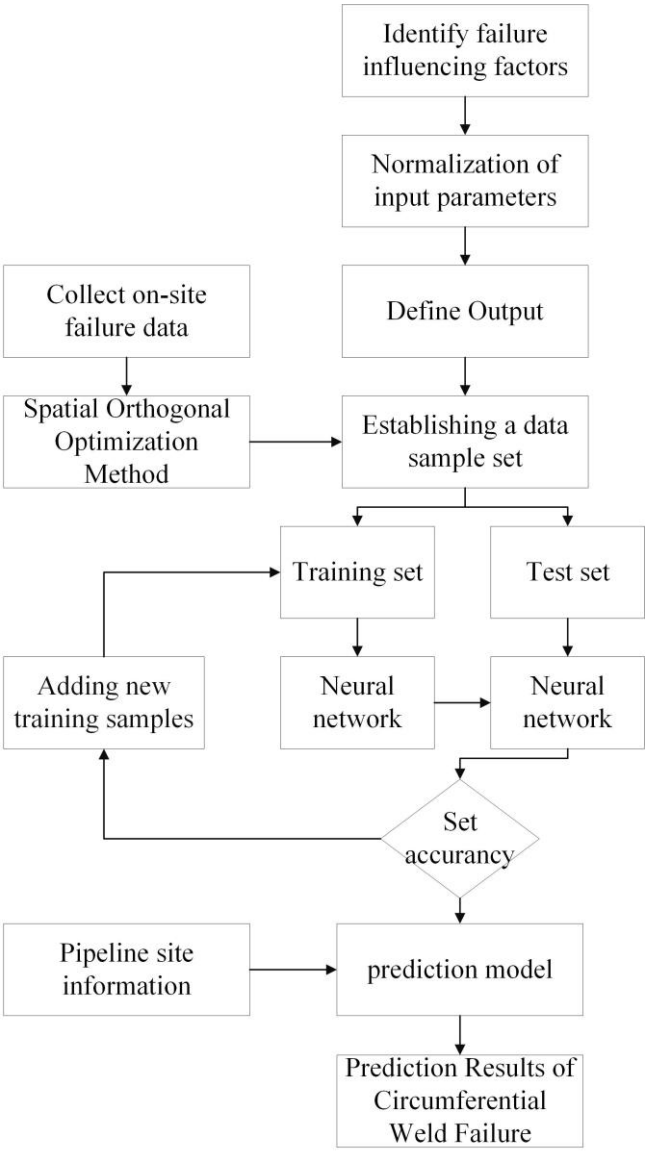

Figure 2. The framework of the research methodology.

4.2. Prediction Model Establishment

The back-propagation (BP) network [33] is a multilayer feed-forward neural network whose neurons are passed as a Sigmoid function, which can achieve any nonlinear mapping from input to output. It is called a BP network because the weights are adjusted using a back-propagation learning algorithm. In the practical application of ANNs, the majority of neural network models use BP networks and their variant forms [21]. A typical BP neural network consists of an input layer, at least one hidden layer, and an output layer. Each layer of the network is composed of neurons, represented by $u = \sum x_i w_i + b$ and $y = f(u)$. x_i represents the neuron input and b represents bias. The f function generally takes the Sigmoid function.

For the prediction of pipeline girth weld failure, the parameters involved are shown in Table 2. The number of neurons in the input layer is the same as the number of dimensions of the input parameters, which is 20. The number of nodes in the failure output layer is 3, which are "high risk", "medium risk", and "low risk".

The number of hidden layers in neural networks and the number of nodes in the hidden layers have a great impact on the prediction performance of networks [34]. If the number is too small, the neural network cannot obtain enough information to solve the prediction problem. If the number is too large, it will not only increase the learning time, but also may have the problem of "overfitting". In practice, a BP neural network is mostly three layers with only one hidden layer. That is, the structure of the neural network for girth weld failure risk prediction can be represented as Figure 3.

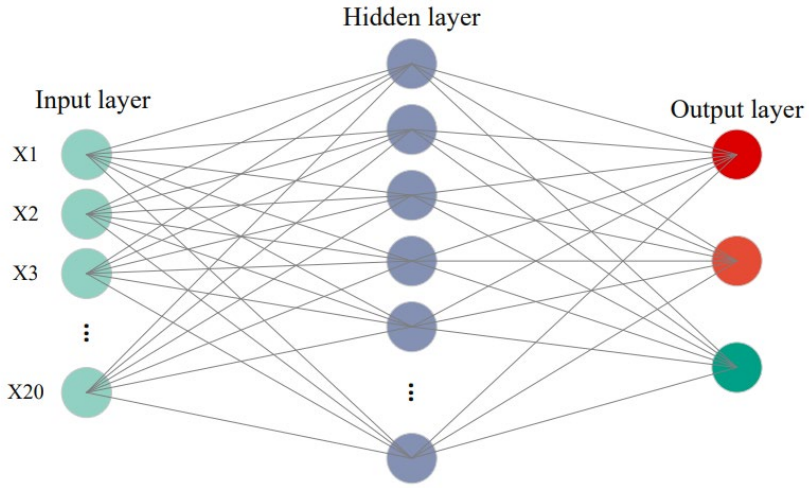

Figure 3. Schematic diagram of the neural network for girth weld failure risk prediction (red circle: high risk; orange circle: medium risk; green circle: low risk).

By selecting the appropriate number of neurons in the hidden layer, the same mapping effect as multiple hidden layers can be achieved. This study adopted a three-layer NN. Before determining the number of hidden-layer neurons, the following speculation is given first:

Speculation 1: As the number of inputs was 20, which was relatively small, the small number of inputs may not fully capture all of the intricate patterns and dependencies present in the data; therefore, a more complex network design is required to effectively model the underlying relationships. The actual network structure required to achieve accurate defect prediction is likely to be more complex than the theoretically optimal network structure.

Speculation 2: For the three-classification pipeline failure risk prediction, the number of hidden layer neurons is in the same order of magnitude as $m \times n$, where m is the input quantity dimension and n is the output quantity dimension.

Also, in order to make the neural network practical, the number of nodes in the hidden layer should be less than $N - 1$ (N is the number of training samples); otherwise, the systematic error of the neural network will tend to 0, independent of the characteristics of the training samples, i.e., the neural network lacks generalization ability. In practice, the number of training samples must be higher than the number of connection weights of the network by 2 to 10 times. When the number of samples is not sufficient, the "rotational training" method is generally used to obtain a reliable neural network. Therefore, the number of neurons in the hidden layer is not only related to the prediction task, but is also related to the number of training samples. In summary, the number of neurons in the hidden layer is recommended to satisfy the following equation.

$$\begin{cases} O(n_1) = O(m \cdot n) \\ n_1 \leq N - 1 \end{cases} \quad (4)$$

where n_1 is the number of neurons in the hidden layer. For the prediction task in this study, m = 20 and n = 3. According to speculations 1 and 2, it can be inferred that the minimum number of hidden layer neurons was 10 and the maximum was 100, i.e., $n_1 \in [10, 100]$.

This interval range was still relatively large. From Equation (4), it can be seen that the search range of n_1 could be further narrowed by determining the number of training samples.

From the perspective of statistics, it can be considered that the probability of selecting the appropriate number of training samples K obeys a normal distribution,

$$f(K) = \frac{e^{-\frac{(K-\mu)^2}{2\sigma^2}}}{\sigma\sqrt{2\pi}} \tag{5}$$

This distribution is usually also denoted as $K \sim N(\mu, \sigma^2)$. From Equation (5), we can derive $\mu \approx 50$. According to the "3σ criteria" in statistics, where almost all values of K are concentrated within the $[\mu - 3\sigma, \mu + 3\sigma]$, $\sigma \approx 10$ can be inferred, i.e., $K \sim N(50, 10^2)$.

Taking a confidence level of 0.9, i.e., the sample size satisfies the training requirement in 90% of cases, one has:

$$P(K < K_{max}) \gg 0.9 \tag{6}$$

where P is the probability function and K_{max} is the maximum number of samples sufficient to train the neural network.

Due to $K \sim N\left(50,\ 10^2\right)$, it follows that

$$\frac{K_{max} - 50}{10} \sim N(0,1) \tag{7}$$

Knowing that $\varphi(1.29) = 0.9015$, then $\frac{K_{max}-50}{10} \approx 1.29$, i.e., $K_{max} \approx 63$. As K obeys a normal distribution, we can get $K_{min} \approx \mu - (K_{max} - \mu) \approx 37$. According to Equation (4), it can be inferred that the number of neurons in the hidden layer is $n_1 \in [10, 35]$. Considering that the output of the network is three categories, n_1 can be roughly determined to be 30 by Speculation 1.

4.3. Training Algorithm

The training process of the BP neural network is mainly divided into two stages; the first stage is the forward propagation of the signal, which passes from the input layer to the hidden layer and finally reaches the output layer; the second stage is the backward propagation of the error, which goes from the output layer to the hidden layer and finally to the input layer, adjusting the weights and biases from the hidden layer to the output layer and the weights and biases from the input layer to the hidden layer in turn. The derivation of the specific training algorithm is shown in Appendix A.

During the training process, the algorithm will analyze the prediction model obtained under the current training sample set. If it reaches the set accuracy, the algorithm will stop; if it fails to reach the set accuracy, new training samples will be added. In this iterative way, the trained model will reach the set classification accuracy. In this iterative way, the training will stop until the trained model reaches the set accuracy.

There are many commonly used formulas for categorization metrics, such as accuracy, precision, recall, etc. Here are the formulas for calculating the common classification metrics based on true positive (TP), false positive (FP), true negative (TN), and false negative (FN):

Accuracy measures the overall correct predictions of the model, accuracy = (TP + TN)/(TP + FP + TN + FN). Recall measures the proportion of correctly predicted positive instances (true positives) out of all actual positive instances, recall = TP/(TP + FN). In this paper, these two are equal; therefore, the term "accuracy" is used consistently throughout.

4.4. Sensitivity Analysis

Sensitivity analysis is a method for studying and analyzing the sensitivity of changes in the state or output of a system (or model) to changes in system parameters or surrounding conditions. Sensitivity analysis is often used in optimization methods to study the stability of the optimal solution when the original data are inaccurate or changes occur. Sensitivity analysis can also be used to determine which parameters have a greater effect on the system or model.

The conventional methods of sensitivity analysis are used by varying a particular input on a fixed basis of all inputs and observing the change in output at that point. However, this method does not work for practical nonlinear mapping systems. In the case of girth weld failure risk prediction, for example, once the material of the pipe is changed, parameters such as the pipe diameter, toughness, and design pressure will also change. Obviously, the sensitivity analysis method that fixes other input values cannot obtain an accurate solution. In this study, the analytical solution of the degree of influence of each input on the risk prediction results is derived from the perspective of mathematical analysis.

As a BP neural network was used in the girth weld failure risk prediction, the sensitivity of the output of the second layer $o_{i_2}^2$ to the input of the input layer $z_{i_1}^1$ can be expressed as:

$$\frac{\partial o_{i_2}^2}{\partial o_{i_1}^1} \cdot \frac{\partial o_{i_1}^1}{\partial z_{i_1}^1} = s\left(z_{i_2}^2\right)\left(1 - s\left(z_{i_2}^2\right)\right) w_{i_1 i_2}^1 = \zeta_{i_2 i_1}^2 \tag{8}$$

The sensitivity of the output of the third layer $o_{i_3}^3$ to the input layer $z_{i_1}^1$ can be expressed as

$$\frac{\partial o_{i_3}^3}{\partial z_{i_1}^1} = \sum_{i_2=1}^{N_2} \frac{\partial o_{i_3}^3}{\partial o_{i_2}^2} \cdot \frac{\partial o_{i_2}^2}{\partial z_{i_1}^1} = \sum_{i_2=1}^{N_2} \frac{\partial o_{i_3}^3}{\partial o_{i_2}^2} \cdot \zeta_{i_2 i_1}^2 = \sum_{i_2=1}^{N_2} s\left(z_{i_3}^3\right)\left(1 - s\left(z_{i_3}^3\right)\right) \cdot w_{i_2 i_3}^2 \cdot \zeta_{i_2 i_1}^2 = \zeta_{i_3 i_1}^3 \tag{9}$$

The sensitivity of the output of the fourth layer $o_{i_4}^4$ to the input layer $z_{i_1}^1$ can be expressed as:

$$\frac{\partial o_{i_4}^4}{\partial z_{i_1}^1} = \sum_{i_3=1}^{N_3} \frac{\partial o_{i_4}^4}{\partial o_{i_3}^3} \cdot \frac{\partial o_{i_3}^3}{\partial z_{i_1}^1} = \sum_{i_3=1}^{N_3} \frac{\partial o_{i_4}^4}{\partial o_{i_3}^3} \cdot \zeta_{i_3 i_1}^3 = \sum_{i_3=1}^{N_3} s\left(z_{i_4}^4\right)\left(1 - s\left(z_{i_4}^4\right)\right) \cdot w_{i_3 i_4}^3 \cdot \zeta_{i_3 i_1}^3 = \zeta_{i_4 i_1}^4 \tag{10}$$

By analogy, it can be inferred that the sensitivity of the output of the layer L to input $z_{i_1}^1$ is:

$$\frac{\partial o_{i_L}^L}{\partial z_{i_1}^1} = \sum_{i_{L-1}=1}^{N_{L-1}} \frac{\partial o_{i_L}^L}{\partial o_{i_{L-1}}^{L-1}} \cdot \frac{\partial o_{i_{L-1}}^{L-1}}{\partial z_{i_1}^1} = \sum_{i_{L-1}=1}^{N_{L-1}} \frac{\partial o_{i_L}^L}{\partial o_{i_{L-1}}^{L-1}} \cdot \zeta_{i_{L-1} i_1}^{L-1} = \sum_{i_{L-1}=1}^{N_{L-1}} s\left(z_{i_L}^L\right)\left(1 - s\left(z_{i_L}^L\right)\right) \cdot w_{i_{L-1} i_L}^{L-1} \cdot \zeta_{i_{L-1} i_1}^{L-1} = \zeta_{i_L i_1}^L \tag{11}$$

The sensitivity of the input parameters on the output results can be calculated by the above equation.

5. Results and Discussion

5.1. Influencing Factor Analysis

Spearman correlation analysis was adopted to determine the correlation between influencing factors and failure risk. Figure 4 shows the correlation coefficients of influencing factors with the failure risk of the girth weld. It can be seen that X1, X3, X4, X5, and X14 showed a negative correlation with the failure risk and others showed a positive correlation. X17 (weld radiographic grade), X16 (defect height), X12 (defect type), X13 (defect position along the depth direction), and X15 (defect length) had relative correlation coefficients with the weld failure risk.

Figure 5 shows the correlation between the influencing factors in different sample categories. The variability of the correlation coefficient matrices was not significant. X1 and X5, X1 and X6, X5 and X6, X12 and X13, X2 and X18, and X16 and X17 showed strong correlations in all samples. Differently, there was a strong correlation between X1, X2, X3, X5, X6, and X7 (all of these belong to pipe material and performance) in the high-risk samples.

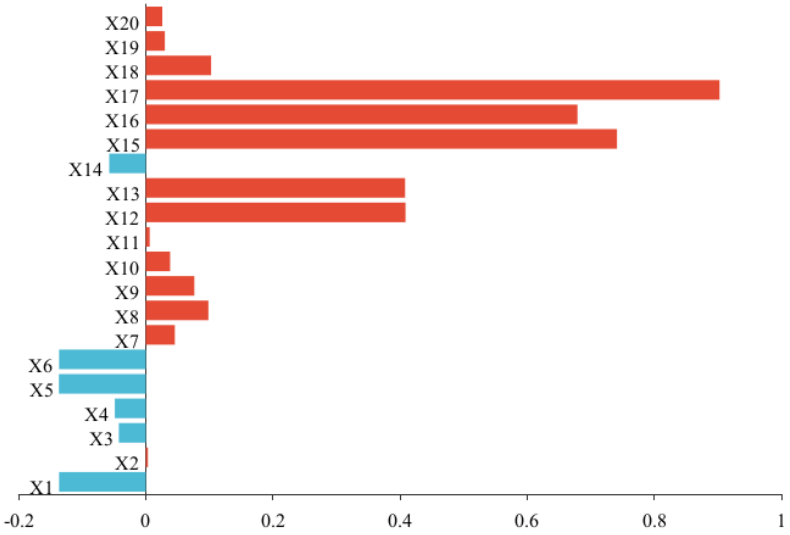

Figure 4. Correlation coefficients of influencing factors with the failure risk of the girth weld.

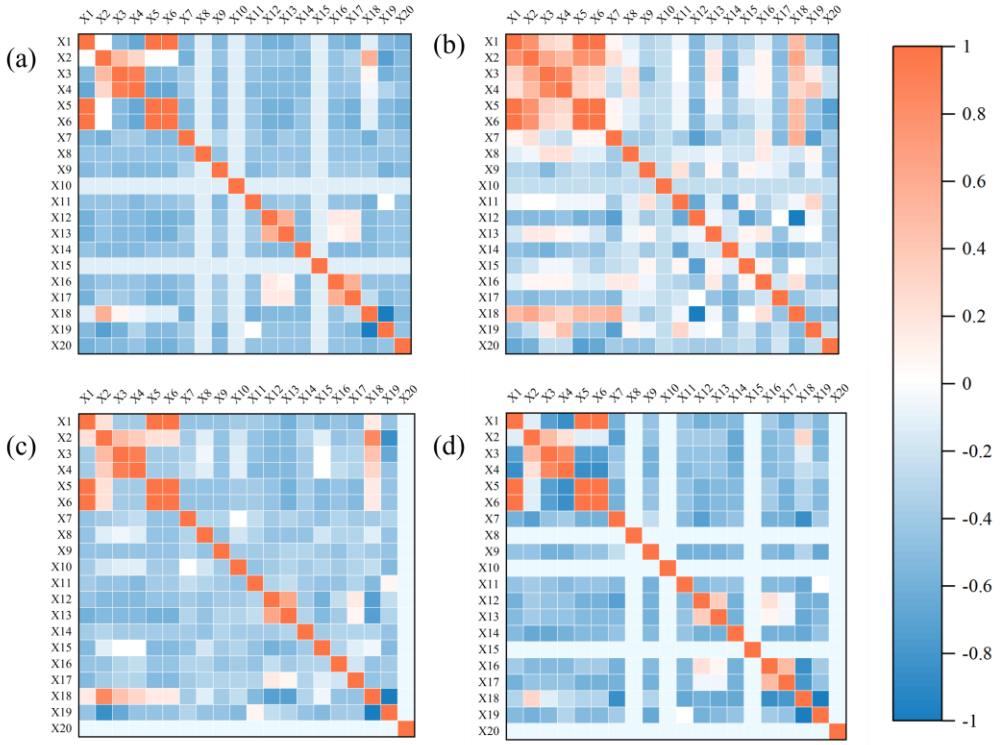

Figure 5. Correlations between the influencing factors in different sample categories. (**a**) All samples; (**b**) high-risk samples; (**c**) medium-risk samples; (**d**) low-risk samples.

5.2. Model Prediction Performance

The BP neural network used in this study contained three layers: an input layer of 20 neurons, a hidden layer of 30 neurons, and an output layer of 3 neurons. In the training process, the initial number of training samples K was set to 10 and the learning rate was set to 0.001. In the training process, the set classification accuracy was 80%. Owing to the initial small number of samples, the training could not reach the set accuracy requirements, and the program analyzed the prediction accuracy of the model for medium-, high-, and low-risk data, respectively. If the prediction accuracy of a certain risk level failed to reach the set accuracy, a new sample corresponding to the risk level was added to the training set and the training would start again. Training did not stop until the model was able to

achieve the set accuracy in the prediction of high, medium, and low risk levels. The final count of training samples consisted of 25 high-risk samples, 247 medium-risk samples, and 330 low-risk samples.

Tables 5 and 6 show the evaluation of the prediction results of the model. It can be seen that, in the presence of an extreme imbalance in the three risk levels of the samples, a relatively accurate failure risk prediction could be achieved using the training sample selection method and neural network architecture established in this study. The prediction accuracy for all risks of girth welds was acceptable. In the case of high-risk welds, the accuracy reached 73.7% with only 25 training samples. For further improving the accuracy of the prediction, a higher accuracy can be set before the training starts, but the higher the accuracy, the more training costs are usually required. Another option is to increase the number of training samples, but the effects of imbalanced data should receive more attention.

Table 5. Prediction results (including training samples) of the neural network for the failure risk prediction of the girth weld.

Risk Level	Correct Identification	Incorrect Identification	Success Rate	Number of Training Samples
High risk	39	5	88.6%	25
Medium risk	1563	260	85.7%	247
Low risk	2533	417	85.9%	330

Table 6. Prediction results (excluding training samples) of the neural network for the failure risk prediction of the girth weld.

Risk Level	Correct Identification	Incorrect Identification	Success Rate	Number of Training Samples
High risk	14	5	73.7%	25
Medium risk	1316	260	83.5%	247
Low risk	2203	417	84.1%	330

5.3. Parameter Sensitivity

Figure 6 shows the sensitivity of the input parameters of the prediction model on the output. The sensitivity of different parameters varied considerably. X15 had the greatest sensitivity, followed by X2, X5, and X4, which meant that the defect length, pipe diameter, yield strength, wall thickness, and defect height had the greatest effect on the change in pipeline failure risk. In contrast, the weld radiographic grade, geological area, repaired or not, steel grade, and toughness had smaller effects on the change in risk. Therefore, the elimination of weld defects during the welding process and the inspection and monitoring of defects during the service life of the pipeline could play an important role in reducing the risks of failure of the girth welds.

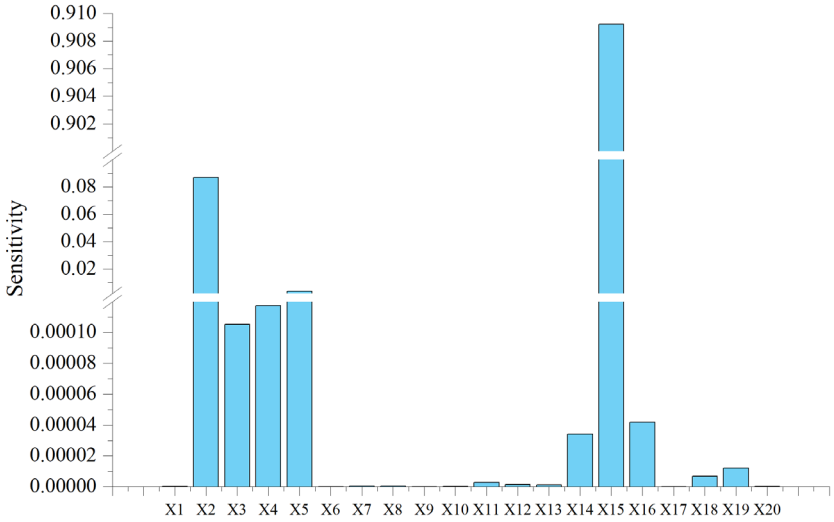

Figure 6. Sensitivity analysis of the input parameters on the output.

6. Conclusions

This study focused on the failure risk of circumferential welds in oil and gas pipelines. Based on the collection of pipeline failure cases and field inspection data, a total of 20 main factors (including 11 pipe-type and performance-related indicators, 6 defect-related indicators, and 3 load-related indicators) affecting the failure risk of the girth welds of pipelines and their normalization methods were identified. The samples were selected by the spatially orthogonal optimal method to effectively avoid the overfitting problem caused by the imbalance of classification samples. Using the BP neural network, a prediction model for the failure risk of girth welds in high-strength steel pipelines was established and the prediction accuracy reached more than 83% (except for high-risk samples), improving the technical support for high-risk girth weld repair and maintenance decisions and avoiding the failure of pipeline girth welds.

The advantage of this method is that it achieved high training accuracy with fewer samples and was better for samples with imbalance sample distributions, but had requirements regarding the quality of the samples themselves and the quality of the distribution. The disadvantage was that there may have been underfitting if the training data were small.

Some factors not included in the model, such as residual stress and the state of the environment inside the pipe, also play an important role in pipeline weld failure. Future research will take these factors into account to build a more accurate and applicable risk prediction model for pipeline girth welds.

Author Contributions: Conceptualization, K.W.; Methodology, K.W.; Software, K.W. and Y.Z.; Validation, W.M.; Formal analysis, Q.G.; Data curation, K.W.; Writing—original draft, K.W.; Writing—review & editing, M.Z., W.M. and W.W.; Visualization, Q.G. and Y.Z.; Supervision, M.Z.; Funding acquisition, W.W. All authors have read and agreed to the published version of the manuscript.

Funding: This research was funded by the Key R&D Plan of Shaanxi Province, China (Grant No. 2022ZDLSF07-08), the Youth Science and Technology New Star Project of Shaanxi Province (Grant No. 2021KJXX65), and the Natural Science Basic Research Program of Shaanxi Province of China (Program No. 2023-JC-YB-447).

Data Availability Statement: The data presented in this study are available on request from the corresponding author.

Conflicts of Interest: The authors declare no conflict of interest.

Appendix A

The overall output error of the neural network for failure risk prediction is

$$\mathrm{E} = \sum_{j_L=1}^{N_L} \left(T_{j_L} - O_{j_L}^L \right)^2 \tag{A1}$$

where L is the number of neural network layers; N_L is the number of neurons in layer L; T_{jL} is the standard output of layer L; and O_{jL}^L is the actual output of layer L. For the neural network of girth weld failure risk prediction, L = 3 and N_1 = 20, N_2 = 30, and N_3 = 3.

Let $w_{j_{L-1}j_L}^L$ represent the weight of the connection between the j-th neuron of the layer L-1 and the j-th neuron of the layer L, then the partial derivative of the error to $w_{j_{L-1}j_L}^L$ can be expressed as

$$\frac{\partial \mathrm{E}}{\partial w_{j_{L-1}j_L}^L} = \frac{\partial \mathrm{E}}{\partial O_{j_L}^L} \cdot \frac{\partial O_{j_L}^L}{\partial z_{j_L}^L} \cdot \frac{\partial z_{j_L}^L}{\partial w_{j_{L-1}j_L}^L} \tag{A2}$$

where the output $O_{j_L}^L$ and the input $z_{j_L}^L$ are sigmoid functions (see Equation (A3)).

$$O_{j_L}^L = \frac{1}{1 + \mathrm{e}^{-z_{j_L}^L}} = \mathrm{s}(z_{j_L}^L) \tag{A3}$$

According to Equation (A3), it can be inferred that

$$\frac{\partial O_{j_L}^L}{\partial z_{j_L}^L} = \mathrm{s}(z_{j_L}^L) \cdot (1 - \mathrm{s}(z_{j_L}^L)) \tag{A4}$$

Then

$$\frac{\partial \mathrm{E}}{\partial O_{j_L}^L} = -(T_{j_L} - O_{j_L}^L) \tag{A5}$$

Due to the fact that the total input of neurons can be expressed as

$$z_{j_L}^L = \sum_{j_{L-1}=1}^{N_{L-1}} w_{j_{L-1}j_L}^L \cdot O_{j_{L-1}}^{L-1} + b_{j_L}^L \tag{A6}$$

It can be introduced that

$$\frac{\partial z_j^L}{\partial w_{j_{L-1}j_L}^L} = O_{j_{L-1}}^{L-1} \tag{A7}$$

Take Equations (A4), (A5), and (A7) into (A2) to get the partial derivative of output layer deviation and weight

$$\frac{\partial \mathrm{E}}{\partial w_{j_{L-1}j_L}^L} = -\left(T_{j_L} - O_{j_L}^L \right) \cdot \mathrm{s}\left(z_{j_L}^L \right) \cdot \left(1 - \mathrm{s}\left(z_{j_L}^L \right) \right) \cdot O_{j_{L-1}}^{L-1} \tag{A8}$$

The partial derivative of the bias can be easily obtained

$$\frac{\partial \mathrm{E}}{\partial b_{j_L}^L} = -\left(T_{j_L} - O_{j_L}^L \right) \cdot \mathrm{s}\left(z_{j_L}^L \right) \cdot \left(1 - \mathrm{s}\left(z_{j_L}^L \right) \right) \tag{A9}$$

Let $\delta_{j_L}^L = -\left(T_{j_L} - O_{j_L}^L \right) \cdot \mathrm{s}\left(z_{j_L}^L \right) \cdot \left(1 - \mathrm{s}\left(z_{j_L}^L \right) \right)$, then

$$\frac{\partial \mathrm{E}}{\partial w_{j_{L-1}j_L}^L} = \delta_{j_L}^L \cdot O_{j_{L-1}}^{L-1} \tag{A10}$$

$$\frac{\partial \mathrm{E}}{\partial b_{j_L}^L} = \delta_{j_L}^L \tag{A11}$$

For the hidden layer $L-1$, the deviation of the error from the output of neurons in the $L-1$ layer can be expressed as

$$\frac{\partial \mathrm{E}}{\partial O_{j_{L-1}}^{L-1}} = \sum_{j_L}^{N_L} \frac{\partial E_{j_L}}{\partial z_{j_L}^L} \cdot \frac{\partial z_{j_L}^L}{\partial O_{j_{L-1}}^{L-1}} = \sum_{j_L}^{N_L} \left(-\left(T_{j_L} - O_{j_L}^L \right) \cdot \mathrm{s}\left(z_{j_L}^L \right) \cdot \left(1 - \mathrm{s}\left(z_{j_L}^L \right) \right) \cdot \frac{\partial z_{j_L}^L}{\partial O_{j_{L-1}}^{L-1}} \right) \tag{A12}$$

From $z_{j_L}^L = \sum_{j_{L-1}}^{N_{L-1}} O_{j_{L-1}}^{L-1} w_{j_{L-1}j_L}^L + b_{j_L}^L$, it can be concluded that

$$\frac{\partial z_{j_L}^L}{\partial O_{j_{L-1}}^{L-1}} = w_{j_{L-1}j_L}^L \tag{A13}$$

Taking Equation (A13) into Equation (A12) yields

$$\frac{\partial \mathrm{E}}{\partial O_{j_{L-1}}^{L-1}} = \sum_{j_L}^{N_L} \frac{\partial E_{j_L}}{\partial z_{j_L}^L} \cdot \frac{\partial z_{j_L}^L}{\partial O_{j_{L-1}}^{L-1}} = \sum_{j_L}^{N_L} \left(-\left(T_{j_L} - O_{j_L}^L \right) \cdot \mathrm{s}\left(z_{j_L}^L \right) \cdot \left(1 - \mathrm{s}\left(z_{j_L}^L \right) \right) \cdot w_{j_{L-1}j_L}^L \right) = \sum_{j_L}^{N_L} \left(\delta_{j_L}^L \cdot w_{j_{L-1}j_L}^L \right) \tag{A14}$$

Then

$$\frac{\partial \mathrm{E}}{\partial w_{j_{L-2}j_{L-1}}^{L-1}} = \sum_{j_L}^{N_L} \left(\delta_{j_L}^L \cdot w_{j_{L-1}j_L}^L \right) \cdot \frac{\partial O_{j_{L-1}}^{L-1}}{\partial z_{j_{L-1}}^{L-1}} \cdot \frac{\partial z_{j_{L-1}}^{L-1}}{\partial w_{j_{L-2}j_{L-1}}^{L-1}} = \sum_{j_L}^{N_L} \left(\delta_{j_L}^L \cdot w_{j_{L-1}j_L}^L \right) \cdot \mathrm{s}(z_{j_{L-1}}^{L-1}) \cdot (1 - \mathrm{s}(z_{j_{L-1}}^{L-1})) \cdot O_{j_{L-2}}^{L-2} \tag{A15}$$

$$\frac{\partial \mathrm{E}}{\partial b_{j_{L-1}}^{L-1}} = \sum_{j_L}^{N_L} \left(\delta_{j_L}^L \cdot w_{j_{L-1}j_L}^L \right) \cdot \mathrm{s}(z_{j_{L-1}}^{L-1}) \cdot (1 - \mathrm{s}(z_{j_{L-1}}^{L-1})) \tag{A16}$$

Similarly, let $\delta_{j_{L-1}}^{L-1} = \sum_{j_L}^{N_L} \left(\delta_{j_L}^L \cdot w_{j_{L-1}j_L}^L \right) \cdot \mathrm{s}\left(z_{j_{L-1}}^{L-1} \right) \cdot \left(1 - \mathrm{s}\left(z_{j_{L-1}}^{L-1} \right) \right)$, and it follows that

$$\frac{\partial \mathrm{E}}{\partial w_{j_{L-2}j_{L-1}}^{L-1}} = \delta_{j_{L-1}}^{L-1} \cdot O_{j_{L-2}}^{L-2} \tag{A17}$$

$$\frac{\partial \mathrm{E}}{\partial b_{j_{L-1}}^{L-1}} = \delta_{j_{L-1}}^{L-1} \tag{A18}$$

Owing to the number of layers in the failure prediction neural network being 3, the back-propagation of errors will reach the $L-2$ layer. The deviation of the output error from the output of $L-2$ layer can be expressed as

$$\frac{\partial \mathrm{E}}{\partial O_{j_{L-2}}^{L-2}} = \sum_{j_{L-1}}^{N_{L-1}} \frac{\partial \mathrm{E}}{\partial O_{j_{L-1}}^{L-1}} \cdot \frac{\partial O_{j_{L-1}}^{L-1}}{\partial O_{j_{L-2}}^{L-2}} \tag{A19}$$

Take $\frac{\partial \mathrm{E}}{\partial O_{j_{L-1}}^{L-1}} = \sum_{j_L}^{N_L} \left(\delta_{j_L}^L \cdot w_{j_{L-1}j_L}^L \right)$ into Equation (A19), then

$$\frac{\partial \mathrm{E}}{\partial O_{j_{L-2}}^{L-2}} = \sum_{j_{L-1}}^{N_{L-1}} \sum_{j_L}^{N_L} \left(\delta_{j_L}^L \cdot w_{j_{L-1}j_L}^L \right) \cdot \frac{\partial O_{j_{L-1}}^{L-1}}{\partial O_{j_{L-2}}^{L-2}} \tag{A20}$$

Considering $\frac{\partial O_{j_{L-1}}^{L-1}}{\partial O_{j_{L-2}}^{L-2}} = \frac{\partial O_{j_{L-1}}^{L-1}}{\partial z_{j_{L-1}}^{L-1}} \cdot \frac{\partial z_{j_{L-1}}^{L-1}}{\partial O_{j_{L-2}}^{L-2}} = \mathrm{s}\left(z_{j_{L-1}}^{L-1} \right) \cdot \left(1 - \mathrm{s}\left(z_{j_{L-1}}^{L-1} \right) \right) \cdot \frac{\partial z_{j_{L-1}}^{L-1}}{\partial O_{j_{L-2}}^{L-2}}$, from $z_{j_{L-1}}^{L-1} = \sum_{j_{L-2}}^{N_{L-2}} O_{j_{L-2}}^{L-2} w_{j_{L-2}j_{L-1}}^{L-1} + b_{j_L-1}^{L-1}$, it can be concluded that

$$\frac{\partial z_{j_{L-1}}^{L-1}}{\partial O_{j_{L-2}}^{L-2}} = w_{j_{L-2}j_{L-1}}^{L-1} \tag{A21}$$

Then

$$\frac{\partial O_{j_{L-1}}^{L-1}}{\partial O_{j_{L-2}}^{L-2}} = \mathrm{s}\left(z_{j_{L-1}}^{L-1} \right) \cdot \left(1 - \mathrm{s}\left(z_{j_{L-1}}^{L-1} \right) \right) \cdot w_{j_{L-2}j_{L-1}}^{L-1} \tag{A22}$$

Introducing Equation (A22) into Equation (A19) includes

$$\frac{\partial \mathrm{E}}{\partial O_{j_{L-2}}^{L-2}} = \sum_{j_{L-1}}^{N_{L-1}} \frac{\partial \mathrm{E}}{\partial O_{j_{L-1}}^{L-1}} \cdot \frac{\partial O_{j_{L-1}}^{L-1}}{\partial O_{j_{L-2}}^{L-2}} = \sum_{j_{L-1}}^{N_{L-1}} \left(\sum_{j_L}^{N_L} \left(\delta_{j_L}^L \cdot w_{j_{L-1}j_L}^L \right) \cdot \mathrm{s}\left(z_{j_{L-1}}^{L-1} \right) \cdot \left(1 - \mathrm{s}\left(z_{j_{L-1}}^{L-1} \right) \right) \right) \cdot w_{j_{L-2}j_{L-1}}^{L-1} \tag{A23}$$

By incorporating $\delta_{j_{L-1}}^{L-1} = \sum_{j_L}^{N_L}\left(\delta_{j_L}^{L}\cdot w_{j_{L-1}j_L}^{L}\right)\cdot \mathrm{s}\left(z_{j_{L-1}}^{L-1}\right)\cdot\left(1-\mathrm{s}\left(z_{j_{L-1}}^{L-1}\right)\right)$ into Equation (A23), the backward error propagation of the neural network can be obtained

$$\frac{\partial \mathrm{E}}{\partial O_{j_{L-2}}^{L-2}} = \sum_{j_{L-1}}^{N_{L-1}} \delta_{j_{L-1}}^{L-1}\cdot w_{j_{L-2}j_{L-1}}^{L-1} \tag{A24}$$

Based on Equation (A23), there are

$$\frac{\partial \mathrm{E}}{\partial w_{j_{L-3}j_{L-2}}^{L-2}} = \frac{\partial \mathrm{E}}{\partial O_{j_{L-2}}^{L-2}}\cdot\frac{\partial O_{j_{L-2}}^{L-2}}{\partial z_{j_{L-2}}^{L-2}}\cdot\frac{\partial z_{j_{L-2}}^{L-2}}{\partial w_{j_{L-3}j_{L-2}}^{L-2}} = \sum_{j_{L-1}}^{N_{L-1}}\left(\delta_{j_{L-1}}^{L-1}\cdot w_{j_{L-2}j_{L-1}}^{L-1}\right)\cdot \mathrm{s}\left(z_{j_{L-2}}^{L-2}\right)\cdot\left(1-\mathrm{s}\left(z_{j_{L-2}}^{L-2}\right)\right)\cdot O_{j_{L-3}}^{L-3} \tag{A25}$$

Similar to $\delta_{j_{L-1}}^{L-1} = \sum_{j_L}^{N_L}\left(\delta_{j_L}^{L}\cdot w_{j_{L-1}j_L}^{L}\right)\cdot \mathrm{s}\left(z_{j_{L-1}}^{L-1}\right)\cdot\left(1-\mathrm{s}\left(z_{j_{L-1}}^{L-1}\right)\right)$, let $\delta_{j_{L-2}}^{L-2} = \sum_{j_{L-1}}^{N_{L-1}}\left(\delta_{j_{L-1}}^{L-1}\cdot w_{j_{L-2}j_{L-1}}^{L-1}\right)\cdot \mathrm{s}\left(z_{j_{L-2}}^{L-2}\right)\cdot\left(1-\mathrm{s}\left(z_{j_{L-2}}^{L-2}\right)\right)$, then

$$\frac{\partial \mathrm{E}}{\partial w_{j_{L-i-1}j_{L-i}}^{L-i}} = \delta_{j_{L-i}}^{L-i}\cdot O_{j_{L-i-1}}^{L-i-1} \tag{A26}$$

$$\frac{\partial \mathrm{E}}{\partial b_{j_{L-2}}^{L-2}} = \delta_{j_{L-2}}^{L-2} \tag{A27}$$

Equations (A26) and (A27) are the error derivations of the backward iterative calculation of the neural network.

References

1. Biezma, M.V.; Andrés, M.A.; Agudo, D.; Briz, E. Most Fatal Oil & Gas Pipeline Accidents through History: A Lessons Learned Approach. *Eng. Fail. Anal.* **2020**, *110*, 104446. [CrossRef]
2. Chen, P.; Li, R.; Fu, K.; Zhao, X. Research and Method for In-Line Inspection Technology of Girth Weld in Long-Distance Oil and Gas Pipeline. *J. Phys. Conf. Ser.* **2021**, *1986*, 012052. [CrossRef]
3. Dai, L.; Wang, D.; Wang, T.; Feng, Q.; Yang, X. Analysis and Comparison of Long-Distance Pipeline Failures. *J. Pet. Eng.* **2017**, *2017*, 3174636. [CrossRef]
4. Guo, Y.; Meng, X.; Wang, D.; Meng, T.; Liu, S.; He, R. Comprehensive Risk Evaluation of Long-Distance Oil and Gas Transportation Pipelines Using a Fuzzy Petri Net Model. *J. Nat. Gas Sci. Eng.* **2016**, *33*, 18–29. [CrossRef]
5. Xia, Y.; Shi, M.; Zhang, C.; Wang, C.; Sang, X.; Liu, R.; Zhao, P.; An, G.; Fang, H. Analysis of Flexural Failure Mechanism of Ultraviolet Cured-in-Place-Pipe Materials for Buried Pipelines Rehabilitation Based on Curing Temperature Monitoring. *Eng. Fail. Anal.* **2022**, *142*, 106763. [CrossRef]
6. Yang, D.; Huang, Y.; Fan, J.; Jin, M.; Peng, Y.; Wang, K. Effect of N2 Content in Shielding Gas on Formation Quality and Microstructure of High Nitrogen Austenitic Stainless Steel Fabricated by Wire and Arc Additive Manufacturing. *J. Manuf. Process.* **2021**, *61*, 261–269. [CrossRef]
7. Zhu, Q.; Chen, J.; Gou, G.; Chen, H.; Li, P. Ameliorated Longitudinal Critically Refracted—Attenuation Velocity Method for Welding Residual Stress Measurement. *J. Mater. Process. Technol.* **2017**, *246*, 267–275. [CrossRef]
8. Sun, J.; Li, C.; Wu, X.-J.; Palade, V.; Fang, W. An Effective Method of Weld Defect Detection and Classification Based on Machine Vision. *IEEE Trans. Ind. Inform.* **2019**, *15*, 6322–6333. [CrossRef]
9. Yang, D.; Cui, Y.; Yu, Z.; Yuan, H. Deep Learning Based Steel Pipe Weld Defect Detection. *Appl. Artif. Intell.* **2021**, *35*, 1237–1249. [CrossRef]
10. Zapata, J.; Vilar, R.; Ruiz, R. Performance Evaluation of an Automatic Inspection System of Weld Defects in Radiographic Images Based on Neuro-Classifiers. *Expert Syst. Appl.* **2011**, *38*, 8812–8824. [CrossRef]
11. Cao, J.; Wang, K.; Ma, W.; Ren, J.; Nie, H.; Dang, W.; Liang, X.; Yao, T.; Zhao, X. Indentation Creep Deformation Behavior of Local Zones for X70 Girth Weld. *Int. J. Press. Vessel. Pip.* **2022**, *199*, 104776. [CrossRef]
12. Xie, M.; Tian, Z. A Review on Pipeline Integrity Management Utilizing In-Line Inspection Data. *Eng. Fail. Anal.* **2018**, *92*, 222–239. [CrossRef]
13. Oliveira, N.; Bisaggio, H.; Netto, T. Probabilistic Analysis of the Collapse Pressure of Corroded Pipelines. In *International Conference on Offshore Mechanics and Arctic Engineering*; American Society of Mechanical Engineers: New York, NY, USA, 2016; Volume 49965, p. V005T04A033.
14. Parvizsedghy, L.; Zayed, T. Consequence of Failure: Neurofuzzy-Based Prediction Model for Gas Pipelines. *J. Perform. Constr. Facil.* **2016**, *30*, 04015073. [CrossRef]
15. Davis, P.M.; Dubois, J.; Olcese, A.; Uhlig, F.; Larivé, J.F.; Martin, D.E. Performance of European Cross-Country Oil Pipelines. *Stat. Summ. Rep. Spillages* **2006**, *54*, 40047961.

16. Liao, K.; Yao, Q.; Wu, X.; Jia, W. A Numerical Corrosion Rate Prediction Method for Direct Assessment of Wet Gas Gathering Pipelines Internal Corrosion. *Energies* **2012**, *5*, 3892–3907. [CrossRef]
17. Parvizsedghy, L.; Zayed, T. Developing Failure Age Prediction Model of Hazardous Liquid Pipelines. In Proceedings of the CSC15—The Canadian Society for Civil Engineering's 5th International/11th Construction Specialty Conference, Vancouver, BC, Canada, 10 June 2015.
18. Su, Y.; Li, J.; Yu, B.; Zhao, Y.; Yao, J. Fast and Accurate Prediction of Failure Pressure of Oil and Gas Defective Pipelines Using the Deep Learning Model. *Reliab. Eng. Syst. Saf.* **2021**, *216*, 108016. [CrossRef]
19. Markowski, A.S.; Mannan, M.S. Fuzzy Logic for Piping Risk Assessment (PfLOPA). *J. Loss Prev. Process Ind.* **2009**, *22*, 921–927. [CrossRef]
20. Shahriar, A.; Sadiq, R.; Tesfamariam, S. Risk Analysis for Oil & Gas Pipelines: A Sustainability Assessment Approach Using Fuzzy Based Bow-Tie Analysis. *J. Loss Prev. Process Ind.* **2012**, *25*, 505–523.
21. Kumari, P.; Halim, S.Z.; Kwon, J.S.-I.; Quddus, N. An Integrated Risk Prediction Model for Corrosion-Induced Pipeline Incidents Using Artificial Neural Network and Bayesian Analysis. *Process Saf. Environ. Prot.* **2022**, *167*, 34–44. [CrossRef]
22. Ren, C.; Qiao, W.; Tian, X. Natural Gas Pipeline Corrosion Rate Prediction Model Based on BP Neural Network. In *Fuzzy Engineering and Operations Research*; Springer: Berlin/Heidelberg, Germany, 2012; pp. 449–455.
23. Li, H.; Ren, X.; Yang, Z. Data-Driven Bayesian Network for Risk Analysis of Global Maritime Accidents. *Reliab. Eng. Syst. Saf.* **2023**, *230*, 108938. [CrossRef]
24. Cai, J.; Jiang, X.; Yang, Y.; Lodewijks, G.; Wang, M. Data-Driven Methods to Predict the Burst Strength of Corroded Line Pipelines Subjected to Internal Pressure. *J. Mar. Sci. Appl.* **2022**, *21*, 115–132. [CrossRef]
25. Chang, Q.; Cao, Y.; Zhen, Y.; Wu, G.; Li, F. Study on the Effect of Loading Conditions on the Fracture Behavior of Pipeline with Girth Weld. *Int. J. Press. Vessel. Pip.* **2023**, *203*, 104940. [CrossRef]
26. Wu, K.; Zhang, D.; Feng, Q.; Yang, Y.; Dai, L.; Wang, D.; Zhang, H.; Guo, G.; Liu, X. Improvement of Fracture Assessment Method for Pipe Girth Weld Based on Failure Assessment Diagram. *Int. J. Press. Vessel. Pip.* **2023**, *204*, 104950. [CrossRef]
27. He, T.; Liao, K.; He, G.; Zhao, J.; Deng, S.; Leng, J. Quantitative Study on Magnetic-Based Stress Detection and Risk Evaluation for Girth Welds with Unequal Wall Thickness of High-Grade Steel Pipelines. *J. Nat. Gas Sci. Eng.* **2022**, *108*, 104825. [CrossRef]
28. Feng, Q.; Sha, S.; Dai, L. Bayesian Survival Analysis Model for Girth Weld Failure Prediction. *Appl. Sci.* **2019**, *9*, 1150. [CrossRef]
29. Feng, Y.; Ji, L.; Chen, H.; Jiang, J.; Wang, X.; Ren, Y.; Zhang, D.; Niu, H.; Bai, M.; Li, S. Research Progress and Prospect of Key Technologies for High-Strain Line Pipe Steel and Pipes. *Nat. Gas Ind. B* **2021**, *8*, 146–153. [CrossRef]
30. Xu, Y.; Wu, M.; Nie, X.; Feng, Z.; Li, L.; Yang, F. Performance Inspection and Defect Cause Analysis of Girth Weld of High Steel Grade Pipeline. *J. Phys. Conf. Ser.* **2022**, *2262*, 012006. [CrossRef]
31. El-Abbasy, M.S.; Senouci, A.; Zayed, T.; Mirahadi, F.; Parvizsedghy, L. Artificial Neural Network Models for Predicting Condition of Offshore Oil and Gas Pipelines. *Autom. Constr.* **2014**, *45*, 50–65. [CrossRef]
32. Xu, W.-Z.; Li, C.B.; Choung, J.; Lee, J.-M. Corroded Pipeline Failure Analysis Using Artificial Neural Network Scheme. *Adv. Eng. Softw.* **2017**, *112*, 255–266. [CrossRef]
33. Shaik, N.B.; Pedapati, S.R.; Taqvi, S.A.A.; Othman, A.R.; Dzubir, F.A.A. A Feed-Forward Back Propagation Neural Network Approach to Predict the Life Condition of Crude Oil Pipeline. *Processes* **2020**, *8*, 661. [CrossRef]
34. Shaik, N.B.; Pedapati, S.R.; Othman, A.R.; Bingi, K.; Dzubir, F.A.A. An Intelligent Model to Predict the Life Condition of Crude Oil Pipelines Using Artificial Neural Networks. *Neural Comput. Appl.* **2021**, *33*, 14771–14792. [CrossRef]